Elongation and Fluctuations of Semiflexible Polymers in a Nematic Solvent

Z. Dogic,[1,*] J. Zhang,[1] A.W.C. Lau,[1] H. Aranda-Espinoza,[3] P. Dalhaimer,[2] D.E. Discher,[2] P.A. Janmey,[3] Randall D. Kamien,[1] T.C. Lubensky,[1] and A.G. Yodh[1]

[1]*Department of Physics and Astronomy, University of Pennsylvania, Philadelphia, Pennsylvania 19104, USA*
[2]*Department of Chemical and Biomolecular Engineering, University of Pennsylvania, Philadelphia, Pennsylvania 19104, USA*
[3]*Institute for Medicine and Engineering, University of Pensylvania, Philadelphia, Pennsylvania 19104, USA*

(Received 13 October 2003; published 24 March 2004)

We directly visualize single polymers with persistence lengths ℓ_p, ranging from 0.05 to 16 m, dissolved in the nematic phase of rodlike *fd* virus. Polymers with a sufficiently large persistence length undergo a coil-rod transition at the isotropic-nematic transition of the background solvent. We quantitatively analyze the transverse fluctuations of the semiflexible polymers and show that at long wavelengths they are driven by the fluctuating nematic background. We extract the Odijk deflection length and the elastic constant of the background nematic phase from the data.

DOI: 10.1103/PhysRevLett.92.125503 PACS numbers: 61.30.–v, 64.70.Md, 82.35.Pq

Polymer coils in solution exhibit a variety of conformational and dynamical behaviors depending on many factors, including polymer concentration, polymer stiffness, solvent quality, solvent flow, and mechanical stress. Exciting recent experiments in this field have focused on disentanglement of single biopolymers in *isotropic* solutions as a result of applied forces and solvent flow [1], and on transport of single biopolymers through networks of barriers [2]. In this Letter, we explore conformations of polymer coils in *anisotropic* solutions. In particular, we present the first direct experimental observations of isolated semiflexible polymers dissolved in a background nematic phase composed of aligned rodlike macromolecules. We show by direct visualization that semiflexible biopolymers dissolved in the nematic phase assume an elongated rodlike configuration aligned with the background nematic director. A coil-rod transition of the biopolymer can thus be induced by causing the solvent to undergo an isotropic-to-nematic (I-N) transition. We quantitatively explore the fluctuations of these semiflexible polymers and find they cannot be described by a theory which treats the nematic background as a fixed external field [3].

Mixtures of semiflexible polymers in lyotropic nematic suspensions exemplify an emerging class of complex fluids — hypercomplex fluids, such as nematic elastomers [4] and nematic emulsions [5], wherein two or more distinct components are combined to create systems that exhibit novel physical properties and functions. Understanding of the polymer-nematic system may lead to new ideas about how to achieve high alignment of biopolymers, complementary to existing methods of DNA alignment [6]. Furthermore, since many biopolymers such as the actin filaments within the sarcomere and neurofilaments within the axon reside in an anisotropic, nematic-like environment [7], our investigation may shed light on organization mechanisms within the cell.

We have used fluorescence microscopy to study four different biopolymers in isotropic and nematic colloidal suspensions. This approach yields new information about dynamics and defects not readily accessible to traditional probes such as x-ray or neutron scattering [8]. In addition, we have developed a rotationally invariant free energy for a single semiflexible polymer in a nematic matrix which generalizes the work in [9,10], and enables us to extract the Odijk length [11] and the elastic constant of the liquid crystal. These first direct measurements of the Odijk deflection length, , allow us to quantify the length scale over which the polymer wanders before it is deflected back by the nematic director.

Our experiments employ an aqueous solution of rodlike *fd* viruses as a background nematic liquid crystal. This system has been studied extensively [12–14], and its phase behavior is well described by the Onsager theory for rods with hard core repulsion [15]. Another advantage of this system is its compatibility with most biopolymers. We use four different semiflexible polymers, whose physical parameters are listed in Table I. To directly visualize the polymers dissolved in the nematic background, we fluorescently labeled each polymer: DNA was labeled with YOYO-1 (Molecular Probes, Eugene, OR), neurofilaments with succinimidyl rhodamine B [20], F-actin filaments with rhodamine-phalloidin (Sigma, St. Louis, MO), and wormlike micelles with PKH26 dye (Sigma, St. Louis, MO) which preferentially partitions into the hydrophobic core of the micelle. Since DNA, neurofilaments, and actin are all negatively charged, we expect

TABLE I. The contour length L, the persistence length ℓ_p, and the diameter a of biopolymers in our experiments.

Polymer	L (m)	ℓ_p (m)	a (nm)	Ref.
-DNA	16	0.05	2	[16]
Neurofilament	2–10	0.2	10	[17]
Wormlike Micelles	5–50	0.5	14	[18]
F-actin	2–20	16	7	[19]
fd virus	0.9	2.2	7	[13]

them to be stable in a suspension of negatively charged *fd* viruses. Wormlike micelles are sterically stabilized with a neutral poly(ethylene oxide) brush layer, which does not interact with the *fd* virus or other proteins [13,18].

Bacteriophage *fd* was grown and dialyzed against a phosphate buffer (150 mM KCl, 20 mM phosphate, 2 mM $MgCl_2$, $p\mathrm{H} = 7.0$) [13]. Samples were prepared by mixing a small amount of polymer with a *fd* solution at different concentrations and were placed between a coverslip and a glass slide. A chamber with a thickness of ~ 50 m was made using a stretched parafilm as a spacer. Samples sealed with optical glue (Norland Products, Cranbury, NJ) were allowed to equilibrate until no drift was visually detectable. To reduce photobleaching, we added an antioxygen solution (2 mg/ml glucose, 360 U/ml catalase, 0.25 vol% mercaptoethanol, 8 U/ml glucose oxidase). All samples were imaged with a fluorescence microscope (Leica IRBE) equipped with a 100 oil-immersion objective and a 100 W mercury lamp. Images were taken with a cooled CCD camera (CoolSnap HQ, Roper Scientific), which was focused at least 5 m away from the surface to minimize possible wall effects.

Figure 1 displays a series of pictures that summarize our qualitative observations. In the nematic phase of *fd*, F-actin [Fig. 1(a)], wormlike micelles [Fig. 1(b)], and neurofilaments [Fig. 1(c)] are highly elongated, having a rodlike shape. By contrast, the same filaments dissolved in an isotropic phase crumple into more compact random coils. Just above the I-N transition, actin filaments and wormlike micelles form hairpin defects [9]. These hairpins exhibit interesting dynamics as shown in Fig. 1(e) and will be explored by us elsewhere. DNA dissolved in *fd* nematic behaves qualitatively differently [Fig. 1(d)]; it forms a slightly anisotropic droplet. Each droplet contains many DNA molecules and, with time, these droplets coalesce into larger droplets. Thus, even at a very low concentration, DNA separates from the *fd* nematic. Taken together, these observations suggest that the persistence length of the polymer is important in determining its solubility in the nematic liquid crystals: DNA has a small ℓ_p and is insoluble, unlike the other stiffer polymers in our experiments. This insolubility may be related to the entropy-driven phase separation of a system of bidisperse rigid rods if their lengths and/or diameters are sufficiently dissimilar [21]. This theory, however, has not been extended to the case of semiflexible polymers.

The large contour lengths of actin filaments and wormlike micelles make them suitable for further quantitative analysis. We focus on the fluctuations of filaments in a background nematic that is free of both defects and distortions. A series of 50 to 100 images were taken with a few seconds between each image to ensure that statistically independent configurations were sampled. For each *fd* concentration, ten filaments were analyzed. The conformation of each polymer was reconstructed by manually marking the end points. [Note that we parametrize

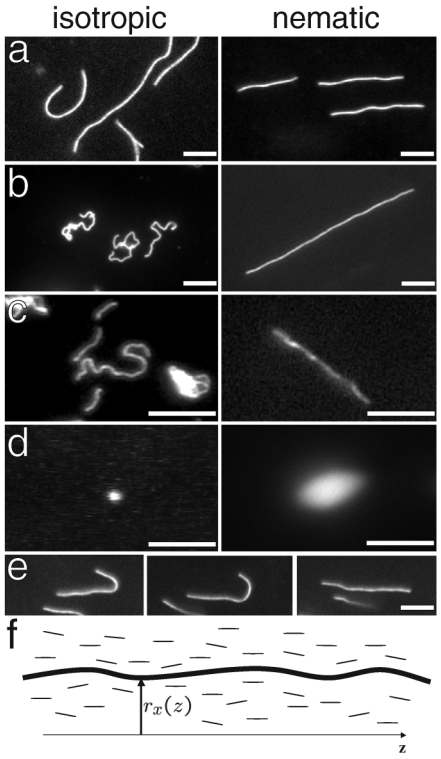

FIG. 1. Images of fluorescently labeled biopolymers in the isotropic (left panels) and nematic (right panels) phases of the *fd* virus. (a)–(d) are, respectively, the images of actin, wormlike micelles, neurofilaments, and DNA. The polymers in an isotropic solution are confined by a thin chamber thus making the samples quasi two dimensional. (e) A sequence of images illustrating an actin filament escaping from a hairpin defect. The scale bar is 5 m. (f) A schematic of a biopolymer in the background nematic field; the conformation of the polymer is parametrized by $\mathbf{R}\ z) = \{r_x\ z\ , r_y\ z\ , z\}$. The nematic director points along the z axis.

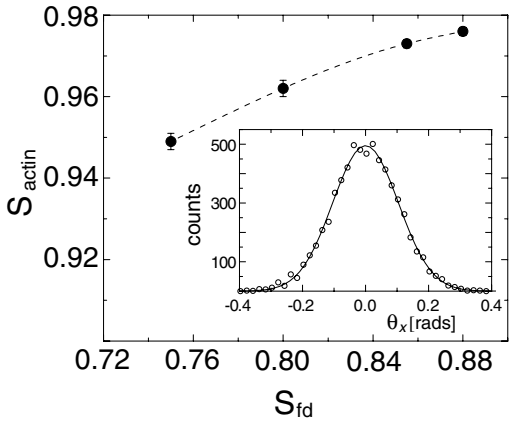

FIG. 2. The order parameter of actin filaments (S_{actin}) vs the order parameter of the background *fd* nematic (S_{fd}). Dashed line is a guide to the eye. The contour length of actin filaments is 15 m or higher. The values of S_{fd} at different *fd* concentrations have been measured in Ref. [14]. Inset: The orientational distribution function (ODF) of actin filaments. The ODF is well approximated by a Gaussian distribution for a wide range of concentrations.

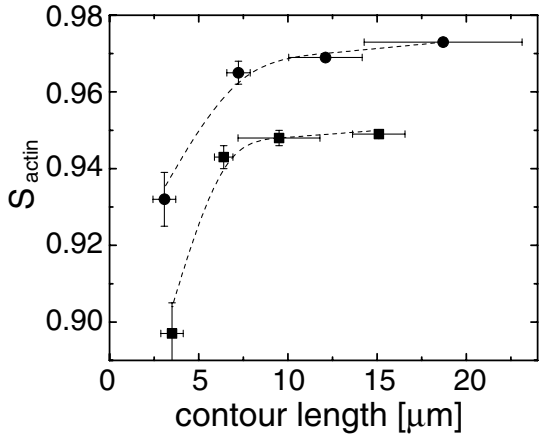

FIG. 3. S_{actin} vs contour lengths of actin. The concentrations of the background nematic *fd* are 41 mg/ml (squares, $S_{fd} = 0.75$) and 28 mg/ml (circles, $S_{fd} = 0.855$). Dashed lines are guides to the eye.

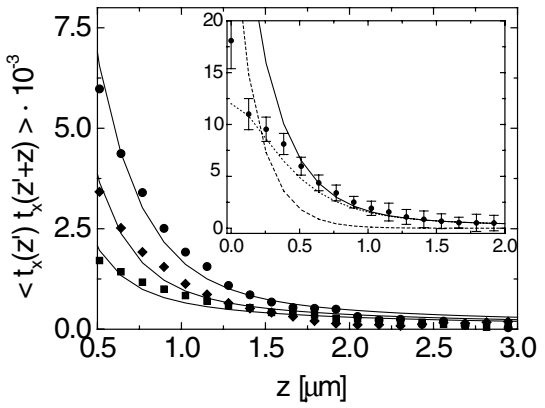

FIG. 4. The x component of the tangent-tangent correlation function for wormlike micelles measured at three different *fd* concentrations (c_{fd}). With *fd* concentration increasing from 39 to 51 to 97 mg/ml the magnitude of the correlation function decreases. The solid lines are theoretical curves generated from Eq. (2) with the best-fit parameters listed in Table II. Inset: TTCF for the lowest concentration of the *fd* virus. The dashed and dotted lines are, respectively, the contributions of the first and second terms in Eq. (2). The data points below 0.5 m are unreliable and have been excluded from the fitting [23].

the transverse deviations of the polymer from the z axis by the 2-component vector $\mathbf{r}\ z$, as shown in Fig. 1(f).] An intensity profile along the x direction for each value of z was extracted. By fitting this intensity to a Gaussian, we obtained subpixel accuracy for $r_x\ z$. We first extracted the orientational distribution function (ODF) from our data. Since our images are two-dimensional projections of the polymer fluctuating in three dimensions, the x component of the tangent vector is measured by $t_x\ z) = \partial\, r_x\ z\ /\partial z \quad {}_x\ z$. The ODF is obtained by creating a histogram of ${}_x$ at different positions along the contour length for a time sequence of 50–100 images. A typical ODF is plotted in Fig. 2; it is well approximated by a Gaussian distribution.

Next, we compute the order parameter of the polymer defined by $S \quad \int_0^L dz \langle 3(\mathbf{t}\ z \quad \hat{z})^2 \quad 1\rangle / 2L) = 1 - 3\langle t_x^2\ 0)\rangle$, where in the last equality, we have used $\langle t_x^2\ z)\rangle = \langle t_y^2\ z)\rangle$. In Fig. 2, we plot S for actin as a function of the background nematic order parameter. It is interesting to observe that S_{actin} is significantly higher than S_{fd}. In order to check that the difference in the alignment between actin and *fd* molecules is due to their different contour lengths, we measured S_{actin} for different contour lengths of actin filaments, as shown in Fig. 3. As the contour length of actin decreases, S_{actin} approaches S_{fd}, as expected intuitively. These observations are qualitatively consistent with the Onsager theory for a bidisperse mixture of rodlike particles with different lengths considered in Ref. [22]. This theory predicts the order parameter of long rods will be higher than the order parameter of the background nematic of shorter rods.

Finally, we measured the tangent-tangent correlation function (TTCF) $\langle t_x\ z'\ t_x\ z' \quad z)\rangle$ for wormlike micelles dissolved in the *fd* virus with concentration 40 mg/ml and larger (Fig. 4). At low *fd* concentrations, the fluctuations of worms are large as evidenced by visual observation of spontaneous formation and dissolution of hairpin defects. In this regime, the measured TTCF does not decay uniformly. We thus focus our analysis on the regime where the background order parameter is very high, and the amplitude of the polymer fluctuations is small. This makes our data suitable for comparison with the theoretical model outlined below.

The fluctuations of a semiflexible polymer in a nematic phase may be described by the free energy [10,24]:

$$F = \frac{k_B T}{2} \int_0^L dz\ \ell_p \left(\frac{\partial \mathbf{t}_\perp}{\partial z} \right)^2 \quad [\mathbf{t}_\perp\ z \quad \mathbf{n}\ 0, z)^2 \quad \frac{1}{2} \int d^3x K (\nabla \quad \mathbf{n})^2, \tag{1}$$

where k_B is the Boltzmann constant, T is the temperature, ℓ_p is the persistence length of the semiflexible polymer, is the strength of the coupling of the polymer to the background nematic field, $\mathbf{n}$ is the local direction of the fluctuating nematic field, and K is the nematic elastic constant. Note that $\mathbf{t}_\perp$ and $\mathbf{n}$ are two-dimensional vectors in the plane perpendicular to the average director. It is straightforward to compute $\langle t_x\ z'\ t_x\ z' \quad z)\rangle$ from Eq. (1):

$$\langle t_x\ z'\ t_x\ z' \quad z)\rangle = \frac{1}{4\ell_p} e^{\ z/\lambda} \quad \frac{1}{8\ {}^2 K\lambda} \int_0^\infty dx \frac{\cos xz/\lambda\ \log 1 \quad D^2/x^2}{1 \quad x^2)[1 \quad x^2 \quad \frac{x^2}{4\pi K} \log 1 \quad D^2/x^2}, \tag{2}$$

TABLE II. The Odijk deflection length , the elastic constant of the background nematic K, and the coupling constant between wormlike micelles and background nematic for different *fd* concentrations obtained from the fits shown in Fig. 4. The best-fit value of ℓ_p of wormlike micelles is 1.5 m.

c_{fd} (mg/ml)	(m)	K (10 ^{8} dyn)	($1/\mu$m)
39	0.18	1.9	46
51	0.13	2.4	88
97	0.06	2.8	416

where $D = 2\pi\lambda/a$ is related to the molecular cutoff which we assume to be the diameter of the polymer ($a \sim 10$ nm). The first term in Eq. (2) describes the fluctuations of a semiflexible polymer in a static external field, with a decaying length set by $= \sqrt{\ell_p/}$. The second term describes the fluctuations of the polymers driven by the tight coupling to the fluctuations of the background nematic field. This term generalizes that of Ref. [10], since it includes the back reaction of the stiff polymer on the nematic fluctuations. Because it decays approximately as a power law, we expect at large length scales the fluctuations of the polymer are always dominated by the nematic fluctuations.

Figure 4 shows our measured TTCF along with the fitted curve of Eq. (2). Overall, good agreement is obtained at distances above 0.5 m [23]. At these distances, most of the fluctuations of the worms are driven by the tight coupling to the background nematic field, coming from the second term in Eq. (2). The best-fit value of ℓ_p is found to be 1.5 m, somewhat higher than those obtained in previous measurements [18]. From the fits to the data, we extract values of the Odijk deflection length , K, and as listed in Table II. We observe that with increasing *fd* concentration, decreases, while K and increase, as one would intuitively expect. Finally, we note that the values for K are in agreement with previous measurements of twist elastic constant $K_{22} = 3$ 10 ^{8} dyn for *fd* samples prepared under similar conditions [25].

In conclusion, we have shown that semiflexible polymers with large enough persistence lengths assume a rodlike conformation when dissolved in a nematic solvent. Using image analysis, a full nematic orientational distribution function was measured. In addition, we have shown that fluctuations of the polymer are driven primarily by the fluctuations of the background nematic field. Direct visualization of individual polymer yields valuable new information about the behavior of polymer chains in anisotropic solvents.

This work was supported by the NSF through Grant No. DMR-0203378 (A. G. Y.), DMR01-29804 (R. D. K.), MRSEC Grant No. DMR-0079909, NASA NAG8-2172 (A. G. Y.), NIH R01 HL67286 (P. A. J.), and the Donors of the Petroleum Research Fund, administered by the American Chemical Society (R. D. K.).

*Current address: Rowland Institute at Harvard, Cambridge, MA 02142, USA.

[1] T. T. Perkins *et al.*, Science **268**, 83 (1995); D. E. Smith *et al.*, Science **283**, 1724 (1999); C. M. Schroeder *et al.*, Science **301**, 1515 (2003); C. Bustamante *et al.*, Nature (London) **421**, 423 (2003).
[2] J. Han and H. G. Craighead, Science **288**, 1026 (2000); D. Nykypanchuk *et al.*, Science **297**, 987 (2002).
[3] M. Warner *et al.*, J. Phys. A **18**, 3007 (1985).
[4] H. Finkelmann *et al.*, Phys. Rev. Lett. **87**, 015501 (2001).
[5] P. Poulin *et al.*, Science **275**, 1770 (1997).
[6] A. Bensimon *et al.*, Science **265**, 2096 (1994); V. Namasivayam *et al.*, Anal. Chem. **74**, 3378 (2002).
[7] R. A. Aldoroty *et al.*, Biophys. J. **51**, 371 (1987); N. Hirokawa *et al.*, J. Cell. Biol. **98**, 1523 (1984).
[8] X. L. Ao and R. B. Meyer, Physica (Amsterdam) **176A**, 63 (1991); M. H. Li *et al.*, Phys. Rev. Lett. **70**, 2297 (1993); J. P. Cotton and F. Hardouin, Prog. Polym. Sci. **22**, 795 (1997).
[9] P.-G. deGennes, in *Polymer Liquid Crystals*, edited by A. Ciferri, W. R. Krigbaum, and R. B. Meyer (Academic, New York, 1982).
[10] R. D. Kamien *et al.*, Phys. Rev. A **45**, 8728 (1992); Phys. Rev. E **48**, 4119 (1993); P. LeDoussal and D. R. Nelson, Europhys. Lett. **15**, 161 (1992).
[11] T. Odijk, Macromolecules **19**, 2313 (1986).
[12] J. Tang and S. Fraden, Liq. Cryst. **19**, 459 (1995).
[13] Z. Dogic and S. Fraden, Philos. Trans. R. Soc. London, Ser. A **359**, 997 (2001).
[14] K. R. Purdy *et al.*, Phys. Rev. E **67**, 031708 (2003).
[15] L. Onsager, Ann. N.Y. Acad. Sci. **51**, 627 (1949).
[16] M. D. Wang *et al.*, Biophys. J. **72**, 1335 (1997).
[17] H. Aranda-Espinoza *et al.* (to be published).
[18] P. Dalhaimer *et al.*, Macromolecules **36**, 6873 (2003).
[19] A. Ott *et al.*, Phys. Rev. E **48**, 1642 (1993); F. Gittes *et al.*, J. Cell Biol. **120**, 923 (1993).
[20] J. F. Leterrier *et al.*, J. Biol. Chem. **271**, 15 687 (1996).
[21] R. van Roij and B. Mulder, J. Chem. Phys. **105**, 11 237 (1996).
[22] H. N. W. Lekkerkerker *et al.*, J. Chem. Phys. **80**, 3427 (1984).
[23] At distances smaller than 0.5 m, we observe a significant deviation of our data from the theoretical curve, which likely arises from the limited spatiotemporal resolution of our microscope. Over the image acquisition time of 250 ms, the fast fluctuations of the polymers at short wavelengths are effectively washed out, leading a lower value in the TTCF. Another possible source of discrepancy is that the spatial resolution of the microscope is smaller than the Odijk deflection length.
[24] J. V. Selinger and R. F. Bruinsma, Phys. Rev. A **43**, 2910 (1991).
[25] Z. Dogic and S. Fraden, Langmuir **16**, 7820 (2000).